A comparative overview of modeling close-encounters in planetary system

Shafiq Ur Rehman
Department of Mathematics, University of Engineering and Technology, Lahore, Pakistan
srehman@uet.edu.pk

(Submitted on 28.04.2021; Accepted on 27.05.2021)

Abstract. N-body simulations of the Sun, the Jovian planets, namely, Jupiter, Saturn, Uranus and Neptune, and smaller bodies, such as moons, asteroids and comets are frequently used to model the orbital evolution of the Solar System. The Sun and planets are represented as massive bodies, whereas the smaller bodies are represented as massless bodies. The Newtonian gravitational attraction between bodies depends on the mass and the distance between the bodies. When the bodies in a simulation consist of the Sun and planets only, no two bodies come close to one another. This is quite different from the case when small bodies, such as asteroids, are included in the simulation, because these bodies can come very close to a planet and even hit the planet. When a small celestial body comes close to a planet, the event is known as a close-encounter. Therefore, an important property of numerical schemes for such simulations is to detect and handle close-encounters accurately. The primary objective of this paper is to discuss potential difficulties to detect close-encounters while performing numerical simulations.

Key words: N-body simulation, Close-encounters, HRC problem, CPU-time

Overview

Astronomy is arguably the oldest of the natural sciences and reflects the history of awareness of mankind in this universe. Key mathematical discoveries in astronomy were Kepler's laws of planetary motion and Newton's formulation of the universal law of gravitation. These laws describe the orbits of planets, asteroids, comets and satellites, and their possible future motion. Sometimes, these motions are very systematic and essentially repeating, as in the case of a planet orbiting the Sun, or the Moon orbiting the Earth; in contrast, sometimes there is seemingly no repetition, as when an asteroid is ejected from the Solar System.

Large numbers of numerical integrators and associated interpolation schemes for performing accurate N-body simulations have been developed and used; see, for example, [Kirsh et al. (2009), Tiscareno & Malhotra (2009), Lykawka et al. (2009), Grazier et al. (1999a), Grazier et al. (1999b), Minton & Malhotra (2010)]. These N-body simulations are performed by first deriving a set of ordinary differential equations (ODEs) for the acceleration, and specifying the initial positions and velocities of the N-bodies at time $t = t_0$. Generally, the initial value problems (IVPs) for N-body simulations are a mixture of first- and second-order ODEs, but the sort of problems we are interested are of the form,

$$y^{''}(t) = f(t, y(t)), \qquad y(t_0) = y_0, \qquad y^{'}(t_0) = y_0^{'}, \tag{1}$$

where $y_0 \in \mathbb{R}^k$ and $y_0^{'} \in \mathbb{R}^k$ denote the initial positions and velocities, respectively, k is the dimension of the IVP, and $f : \mathbb{R} \times \mathbb{R}^k \to \mathbb{R}^k$ is a sufficiently smooth function.

A simple detection scheme is to calculate the distance between the small body and a planet: if the distance is less than the radius of an imaginary

sphere (discussed in Section 1), then the small body is said to have made a close-encounter. There are several definitions for the imaginary sphere, the most commonly used being the Sphere of influence and Hill's sphere. We refer to these spheres as close-encounter spheres. The details about close-encounter spheres are discussed in Section 1.

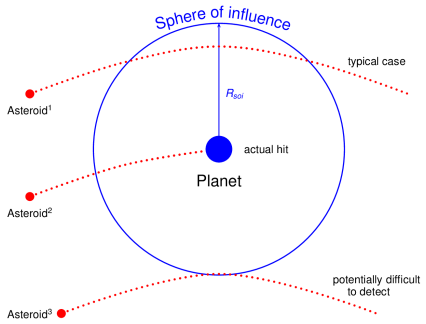

Fig. 1. The close-encounters of an asteroid with a planet, where the planet is at the centre of the sphere with radius R_{soi}.

Fig. 1 depicts an asteroid making close-encounters to a planet, where the planet is placed at the centre of a sphere having radius R_{soi}. Fig. 1 illustrates three cases of close-encounters. The first, illustrated by Asteroid^1, is the most typical case, where the trajectory of the asteroid lies well inside the sphere of influence. The second possibility is illustrated by Asteroid^2, which has collided with the planet. The third case, illustrated by Asteroid^3, is potentially difficult to detect as a close-encounter, because the trajectory of the asteroid is just touching the sphere of influence.

The acceleration of the small body undergoing a close-encounter is dominated by that due to the planet. Since the acceleration depends inversely on the square of the distance, the magnitude of the acceleration varies considerably during a close-encounter, necessitating a large variation in the integration time-step h. This variation can lead to an inefficient simulation unless care is taken. For example, in a simulation of the Sun, Jupiter and an asteroid, suppose that the asteroid had a close-encounter with Jupiter and h was reduced to $h/100$ for both the asteroid and for Jupiter. This wastes computer time, because to a very good approximation, and one that is often used in accurate N-body simulations, asteroids and other small bodies are too small to affect the motion of the planets. Hence, computational time could potentially be saved if the original time-step h was retained for Jupiter.

Several computational time-saving schemes have appeared in the literature; see, for example, [Chambers & Migliorini (1997), Grazier et al. (2008), Grazier et al. (2007), Duncan et al. (1998)]. These schemes depend strongly on whether the integrator used to advance the position of the Sun, planets and small bodies

is symplectic or non-symplectic. Symplectic integrators are special numerical methods that inherit the property of symplecticness when applied to Hamiltonian systems; see, for example, [Calvo & Sanz-Serna (1994)]. The numerical approximations obtained using fixed time-step symplectic integrators exhibit special properties for an exponentially long interval $O(e^{1/h})$. For example, in the absence of round-off error, symplectic integrators have the advantage of ensuring that the error in the energy remains bound; see, for example, [Calvo & Sanz-Serna (1994), Candy (1991), Hairer et al. (2002)], and the error in the dependent variable is linear, compared to a quadratic error growth for non-symplectic integrators. Except for very large t, non-symplectic integrators have the advantage of producing numerical solutions with a smaller error in the position and velocity than for symplectic integrators, provided h is sufficiently small.

A general scheme for handling close-encounters is the following. Suppose an asteroid begins a close-encounter at $t = t_a$ and finishes the close-encounter at $t = t_b$. Let y_1 denote the position of the Sun and the planets, y_2 the position of the small body undergoing the close-encounter, and let z be the position of the Sun and planets that is obtained by continuous approximation. The original system (1) restricted to just the Sun, the planets, and the asteroid is then written as

$$\begin{aligned} y_1'' &= f_1(t, y_1), \\ y_2'' &= f_2(t, y_2, z). \end{aligned} \tag{2}$$

A numerical solution to the y_1-system at $t = t_a + h$ is found by taking a time-step of size h. The y_2-system is then integrated from t_a to $t_a + h$ using time-steps no larger than h. This integration will require the position of the Sun and planets for $t \in (t_a,\, t_a + h)$. The position, in general, is not available from the integration of the y_1-system and is found by interpolation (continuous approximation). This involves fitting a polynomial or piecewise polynomial to the position, and optionally the velocity and acceleration, and evaluating the polynomial at the required time t, with $t_a \leq t \leq t_a + h$.

Specific schemes of the above type have been used; see, for example, [Chambers & Migliorini (1997), Grazier et al. (2008), Grazier et al. (2007), Duncan et al. (1998)]. The order of the continuous approximation should, with one notable exception, be compatible with the order of the integrator. For example, for an integrator of order p, there should be an interpolation polynomial of the same order for a sufficiently accurate approximation to the positions, velocities, and possibly accelerations of the massive bodies and the massless bodies; see, for example, [Rehman (2014)]. The notable exception occurs for high order Störmer methods when used with small step-sizes. The order of the continuous approximation can be significantly less than the order of the Störmer method [Grazier et al. (2013)].

The main requirements of the local interpolants is that they be sufficiently accurate, both when approximating the orbits of the massive bodies, and when approximating the orbits of the massless bodies. In the former case, accurate approximations of the positions and velocities of the massive bodies at any $t \in [t_{n-1}, t_n]$ is important as reduced accuracy at these points (relative to the accuracy associated with the mesh-points) will result in larger errors than expected when evaluating the differential equations that define the trajectories

and energies associated with the massless bodies. For an integration that is order p, the local interpolant should also be order p to ensure that the calculated accuracy of the positions and velocities of the massless bodies are consistent with those of the massive bodies. On the other hand, the local interpolation used when integrating the massless bodies must also be accurate, as these interpolants are used to determine accurate approximations of the "times of the close-encounters" as well as approximations to the position and velocity at the time of the close-encounters.

The interpolation error for a polynomial of degree p can be written as

$$\alpha h^{p+1} \frac{y_{\text{true}}^{(p+1)}(\xi)}{(p+1)!} \ , \tag{3}$$

where y_{true} is the function being approximated, α is a constant, and ξ lies in the interval over which the polynomial is applied. This expression, as is, cannot be used for analysis because the true solution y_{true} is unknown for general N. Another difficulty with expression (3) is that it assumes the data used to form the polynomial is exact. This assumption does not hold for N-body simulations because, for example, the position of a planet at the end of several consecutive steps, will contain errors from the integration. The integration error grows as $t^{3/2}$ for some integrators and as t^2 for others [Brouwer (1937), Grazier et al. (2005a), Grazier et al. (2005b), Hairer et al. (2008)]. In contrast, the interpolation error does not grow with t, so that the interpolation error will become insignificant for sufficiently large t. As soon as this happens, the interpolation method is inefficient because it is too accurate. For planetary orbits, the interpolation error typically decreases with increasing p. This means that the efficiency of the interpolation can be improved by decreasing p with t. The dependence of p on t will both complicate and simplify the analysis. The complication comes from having to analyse different polynomials. The simplification comes from low-degree polynomials being easier to analyse than high-degree polynomials.

1 Background

All the interactions between the massive and the massless bodies are through the Newtonian gravitational forces. This gravitational influence can be approximated as an imaginary sphere centred on the particular planet. We use the most common definitions for the imaginary spheres and refer to them, as noted previously, as close-encounter spheres. Here, we present an overview of these close-encounter spheres.

1.1 Sphere of influence

One definition of the imaginary sphere is the sphere of influence, which is based on a balance of perturbing forces. Consider a system of three bodies: the Sun with mass M at the origin, a planet with mass m at position (x_p, y_p, z_p), and a test particle with negligible mass at position (x_t, y_t, z_t), as shown in Fig. 2. Here, the Sun is at the centre of this coordinate system, which is known as

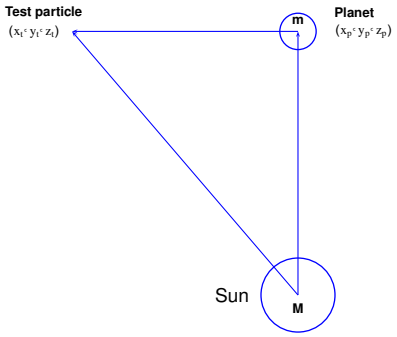

Fig. 2. System of three bodies: the Sun, a planet and a test particle.

the heliocentric frame (for simplicity we have taken the heliocentric coordinate system but this idea also applies to other origins, for example, the centre of mass). The test particle is said to be in the heliocentric region if it is far from the planet, so that the main gravitational force will be that due to the Sun and the planet may be considered as a perturbing body. Otherwise, the test particle is said to be in the planetocentric region, where the planetary attraction will be greater than the solar attraction, so that the Sun should be considered as the perturbing body.

Whether the test particle is in the heliocentric or planetocentric region depends upon the ratio between the total disturbing force and the appropriate central attraction. The boundary of the imaginary sphere is, therefore, the surface on which the ratio of the total disturbing force with the planet's central attraction is equal to that of the Sun. Hence, we must have

$$\frac{||\vec{F}_1'||_2}{||\vec{F}_1||_2} = \frac{||\vec{F}_2'||_2}{||\vec{F}_2||_2}, \tag{4}$$

where $||.||_2$ denotes the L_2-norm and $\vec{F}_1'$ and $\vec{F}_2'$ are the disturbing forces of the heliocentric and planetocentric orbits, respectively, and $\vec{F}_1$ and $\vec{F}_2$ are the Solar and planetary attractions, respectively. The solution of equation (4) gives the radius R_{soi} of the sphere of influence. An approximation of R_{soi} can be obtained using

$$R_{soi} = a\left(\frac{m}{M}\right)^{2/5},$$

where a is the semi-major axis of the planet's orbit and $\frac{m}{M}$ is the ratio of planetary and Solar masses (for detailed calculations see [Danby (1988)]).

1.2 Hill's sphere

A second definition of the imaginary sphere is the Hill's sphere, which is a region around the planet in which the planetary attraction prevents the test

particle from moving into the heliocentric orbit. The region is calculated using the equations of motion of the circular restricted three-body problem, a special problem in which two of the bodies move in a circular orbit and the mass of the third body is assumed negligible. The three-body problem is solved in rotating Cartesian coordinates with the (x, y)-plane in the plane of motion of the two massive bodies and the x-axis along their line of centres. The equations of motion of the massless body in (x, y, z)-space are given as

$$\begin{aligned} x^{''} - 2y^{'} - x = & \quad -\mu_1 \frac{x+\mu_2}{r_1^3} - \mu_2 \frac{x-\mu_1}{r_2^3}, \\ y^{''} + 2x^{'} - y = & \quad -\mu_1 \frac{y}{r_1^3} - \mu_2 \frac{y}{r_2^3}, \\ z^{''} = & \quad -\mu_1 \frac{z}{r_1^3} - \mu_2 \frac{z}{r_2^3}, \end{aligned} \tag{5}$$

where μ_1 and μ_2 are the masses of the two main bodies, scaled so that $\mu_1+\mu_2 = 1$, and $r_1^2 = (x+\mu_2)^2 + y^2 + z^2$, $r_2^2 = (x-\mu_1)^2 + y^2 + z^2$.

By making various assumptions, the system of equations of motion of the test particle in relation to the planet reduces to what are known as Hill's equations [Murray & Dermott (1999)],

$$\begin{aligned} x^{''} - 2y^{'} = & \quad (3 - \frac{\mu_2}{r_2^3})x, \\ y^{''} + 2x^{'} = & \quad -\frac{\mu_2}{r_2^3} y. \end{aligned} \tag{6}$$

The Hill's sphere radius R_H is the distance at which the radial forces vanishes, i.e, at this distance, the Solar tide and mutual attraction are in equilibrium in Hill's equations [Murray & Dermott (1999)]. Different approximations are used to obtain the radius of the Hill's sphere. To have consistency with the definition for the radius of the sphere of influence, we use

$$R_H = a \left(\frac{m}{M}\right)^{1/3}.$$

Table 1. The radii (in A.U.) of the close-encounter spheres of the Jovian planets

Sphere	Jupiter	Saturn	Uranus	Neptune
Sphere of influence: R_{soi}	0.322258	0.364620	0.346036	0.579209
Hill's sphere: R_H	0.512331	0.628208	0.675749	1.118706

Table 1 lists the radii of close-encounter spheres of the Jovian planets [Rehman (2013)], calculated using the data obtained from Williams (2019) and expressed in astronomical units (1 A.U. = 149597870 km). Table 1 shows that $R_{soi} < R_H$ for all four Jovian planets and the radius of Jupiter's sphere of influence is the smallest, while that of Neptune's Hill's sphere is the largest. We also observe from Table 1 that R_H monotonically increases with distance of the Jovian planets to the Sun but R_{soi} is non-monotonic.

2 Close-encounter error

To illustrate the error in a single close-encounter detected during a simulation, consider a planet at the centre of the sphere of influence with radius R_{soi}, as sketched in Figure 3, and suppose we use three different combinations of integrators and interpolation schemes in the main algorithm. Their integration time-steps are denoted by a small circle, a triangle, and a cross, respectively. The three combinations will result in three slightly different orbits, but we used a single trajectory in Fig. 3; the difference between orbits is insignificant

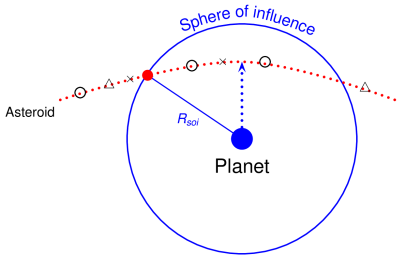

Fig. 3. An illustration of error in a single close-encounter detected during a simulation. The integration time-steps of three different combinations of the main algorithm are denoted by symbols: a small-circle, a triangle, and a cross, respectively.

compared to the radius of the sphere of influence for our purposes here.

Consider the orbit generated by the combination denoted by the small circle. The end of two time-steps is well inside the sphere of influence. The distances between the planet and the asteroid at the end of the time-steps inside the sphere of influence are less than the radius of the sphere of influence and the close-encounter is reported. Next, consider the orbit approximation corresponding to time-steps denoted by a cross. The end of one time-step is inside the sphere of influence, which we also report as a close-encounter. Finally, consider the third orbit associated with the triangles. This orbit takes a large time-step and the end of the step does not lie inside the sphere of influence. Hence, we would miss the close-encounter for this orbit.

Even though two of the three orbit approximations would report a close-encounter, there is likely to be a difference in the time of the close-encounter. There should be a unique time of close-encounter to quantify which of these solutions has to be chosen for the time of close-encounter. In order to ensure fair comparisons between different combinations of the main algorithm, we need to define a unique time of close-encounter.

One possibility is to take the distance between the planet and the asteroid exactly equal to the radius of the sphere of influence and record the corresponding time this equality first occurs as the time of close-encounter.

Physically, there is also a unique global minimum distance between the planet and the asteroid for a single close-encounter. So, another possibility is to take this global minimum distance. For both possibilities, we use a non-linear equation solver (NLES) and an interpolation scheme to find an approximation of the time of close-encounter. As far as the second possibility is concerned, it has the disadvantage that the close-encounter is recorded as soon as the time-step lies inside the sphere of influence, which may be before the point of minimal distance. Hence, the second definition may require extrapolation, or the need to integrate the asteroid further for one or more time-steps, in a post-process routine that stores all this information. This particular situation is illustrated in Fig. 3, for the combination denoted by a small circle: two time-steps lie inside the sphere of influence, one before and the other after the point of minimal distance.

3 Test problem

As is the case for the system of ODEs (1), many problems are independent of the first derivative of their solution and are also independent of time. These types of IVPs are known as autonomous second-order systems of ODEs. We now consider a test problem of this type, namely, the Helin-Roman-Crockett (HRC) problem consisting of the Sun, the Jovian planets and a comet.

3.1 Helin-Roman-Crockett problem

The Helin-Roman-Crockett (HRC) problem models the HRC comet having multiple close-encounters with Jupiter, during which the comet actually orbits Jupiter. The last such close-encounter was observed in 1976 and the comet is

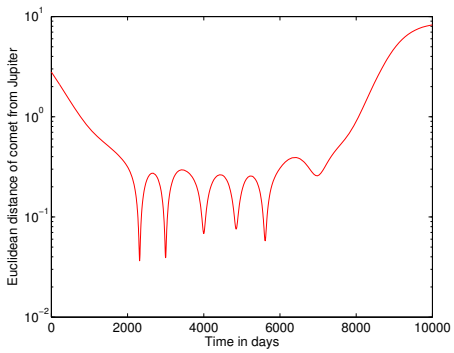

Fig. 4. The distance of the comet from Jupiter in the HRC problem.

expected to make another close-encounter in the year 2075, during which it will be temporarily captured by Jupiter. This temporary capture has been modeled by researchers; see for example, Levison and Duncan (1994). The

equations of motion for the HRC problem are the same as those for the Jovian problem [Rehman (2013)] with the addition of the following equations for the comet at position $\bar{r}_6$:

$$\bar{r}_6''(t) = \sum_{i=1}^{5} \frac{\mu_i(r_i(t) - \bar{r}_6(t))}{||r_i(t) - \bar{r}_6(t)||_2^3} \ . \tag{7}$$

Here, the symbol $\bar{r}$ is used instead of r to indicate that the comet is treated as a massless body. The initial conditions of the comet are given in the Appendix. Figure 4 shows the distance of the comet to Jupiter over a time interval from $t = 0$ to $t = 10,000$ days. The experiment is performed to examine the possible number of close-encounters when the comet comes to a certain distance from Jupiter. The graph clearly shows five close-encounters where the comet comes to within 10^{-2} distance from Jupiter. The figure indicates a possible sixth close-encounter at $t \approx 7000$ days, but the minimum distance to Jupiter is significantly larger than the other five local minima. Hence, this sixth local minimum is often not regarded as a close-encounter.

Figure 5 shows the two-dimensional phase portrait for the components of the position of the comet from $t = 2000$ to $t = 6000$ days. Here, Jupiter lies at the origin. The plotted trajectory is reminiscent of the petals of a flower; due to this similarity, such plots are often referred to as petal plots or tulip diagrams.

The time-step plays a vital role in close-encounters. For example, the close-encounter of Asteroid[3] in Fig. 1 could easily be missed if the time-steps were too large and the distance between planet and test particle was calculated only at the end of the time-steps. The time-step must also be reduced because the magnitude of acceleration increases as the asteroid approaches the planet. Fig-

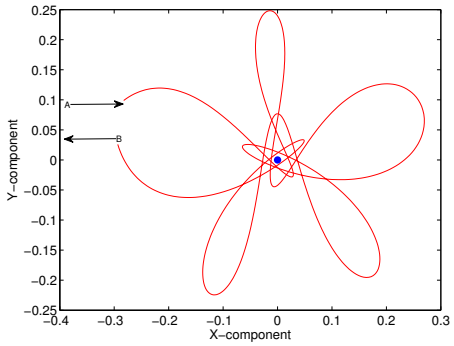

Fig. 5. The two-dimensional phase portrait for the x- and y-components of the position of the comet relative to Jupiter (blue dot) in the HRC problem. Plotted is the orbit segment from $t = 2000$ (A) to $t = 6000$ days (B).

ure 6 shows the step-size sequence for $t \in [0, 10000]$ for different variable-step-

size integrators, *ERKN689* (Explicit Runge-Kutta-Nyström, nine stage, 6-8 pair [Dormand et al. (1987)]), *ERKN81013* (Explicit Runge-Kutta-Nyström, thirteen stage, 8-10 pair [Sharp & Qureshi (2013)]), *ERKN101217* (Explicit Runge-Kutta-Nyström, seventeen stage, 10-12 pair [Dormand et al. (1987)]), and the *ODEX2* integrator [Hairer et al. (1993)]. The maximum step-sizes taken by *ERKN689*, *ERKN81013*, *ERKN101217*, and *ODEX2* are approximately 19.98, 70.82, 157.99, and 408.02 days, respectively. The integrations are performed in double precision using FORTRAN with a local error tolerance of 10^{-14}. We have taken a time interval of 10,000 days to illustrate that the step-

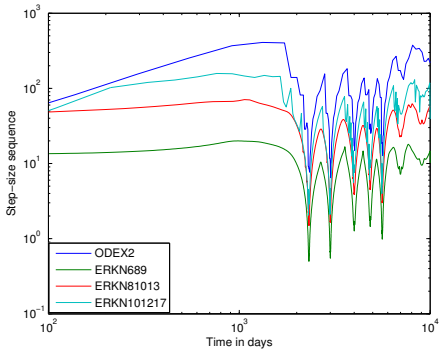

Fig. 6. The step-size sequence versus time using the integrators *ERKN689*, *ERKN101217* and *ODEX2* on the HRC problem.

size decreases significantly as the comet makes close-encounters with Jupiter. The biggest step-size variation has been observed with *ODEX2*, where it reduces from approximately 408.02 days to 7.6 days during one close-encounter. These experiments were performed to illustrate the effect of close-encounters on the step-size.

Conclusion

The main objective of this paper was to discuss potential difficulties to detect close-encounters while performing N-body simulations of the Solar System. An important property of numerical schemes for such simulations is to detect and handle close-encounters accurately. In this paper, we discussed a general scheme for handling close-encounters. The interpolation schemes play a vital role for these kind of simulations. The accurate approximation of the orbits of the massive bodies at any time t is important, because the accuracy influences the accuracy of the orbits of the massless bodies. Similarly, it is equally important to use an appropriate interpolation scheme to obtain accurate approximations of the times of the close-encounters, as well as to the positions and velocities of both the massive and massless bodies at the times of close-encounters. We also presented an overview of close-encounter spheres. We an-

alyzed and compared the radii of the close-encounter spheres of the Jovian planets. In order to ensure fair comparisons between different combinations of integrators and interpolation schemes, there should be a unique time of close-encounter. Therefore, we illustrated different possibilities of close-encounter error in a single close-encounter detected during a simulation. Our numerical testing involved different numerical schemes on a more realistic HRC problem consisting of the Sun, the Jovian planets and a comet.

Acknowledgment

We are grateful to the reviewer for their valuable suggestions to improve the quality of the article.

Appendix

Table 2. Rows 1 to 6 are the initial positions and Rows 7 to 12 are the initial velocities for the HRC problem

	x	y	z
Sun	$0.666919856444077\times10^{-2}$	$-0.723511466440839\times10^{-3}$	$-0.113065442378779\times10^{-3}$
Jupiter	$-0.4929481880506559\times10^{1}$	$-0.2310910532399841\times10^{1}$	$0.1197889941614212\times10^{0}$
Saturn	$-0.5559462159881659\times10^{1}$	$0.7217090743352659\times10^{1}$	$0.1008764843911512\times10^{0}$
Uranus	$-0.1051479684851656\times10^{2}$	$-0.1555904864202644\times10^{2}$	$0.774039048494362\times10^{-1}$
Neptune	$0.1636130229890141\times10^{1}$	$0.2982856616501356\times10^{2}$	$-0.6473579962266688\times10^{0}$
Comet	$-0.3965267044277659\times10^{1}$	$0.3060320798461592\times10^{0}$	$0.2949122108880113\times10^{0}$
Sun	$-0.1597551822288177\times10^{-5}$	$0.7254098157790906\times10^{-5}$	$-0.3038348598973975\times10^{-7}$
Jupiter	$0.3109433296611612\times10^{-2}$	$-0.6477134819096109\times10^{-2}$	$-0.4357172559451174\times10^{-4}$
Saturn	$-0.4717678753258388\times10^{-2}$	$-0.3413503592855709\times10^{-2}$	$0.2469252827795303\times10^{-3}$
Uranus	$0.3227888778570112\times10^{-2}$	$-0.2386568620156909\times10^{-2}$	$-0.5061978789868374\times10^{-4}$
Neptune	$-0.3152327294479188\times10^{-2}$	$0.1931132154044109\times10^{-3}$	$0.6952342277721326\times10^{-4}$
Comet	$-0.1800219023380088\times10^{-2}$	$-0.8521337694196810\times10^{-2}$	$0.1052106206437703\times10^{-3}$

References

Brouwer D., 1937, *Astronomical Journal, p.149–153, 46*
Dormand J., El-Mikkawy M. E. A., Prince P., 1987, *IMA J. Numer. Anal., p.423–430, 7*
Danby J. M. A., 1988, *Richmond, Virginia:Willmann-Bell*
Grazier K. R., Newman W. I., Hyman J. M., Sharp P. W., (2005), *In proc. of 12th Computational Techniques and Applications Conference CTAC-2004, R. May and A. J. Roberts, Eds ANZIAM., p.1086–1103, 46*
Grazier K. R., Newman W. I., Kaula W. M., Hyman J. M., 1999, *ICARUS 140, p.341–352, 2*
Hairer E., McLachlan R. I., Razakarivony A., 2008, *BIT Numerical Mathematics, p.231–243, 48*
Calvo M. P., Sanz-Serna J. M., 1994, *Chapman and Hall, London*

Chambers J. E., Migliorini F., 1997, *Bull. American Astron. Soc, 1024, 29*
Grazier K. R., Dones L., Sharp P. W., 2007, *American Astronomical Society, DDA meeting*
Grazier K. R., Newman W. I., Hyman J. M., Sharp P. W., Goldstein D. J., 2005, *In Proc. of 12th Computational Techniques and Applications Conference CTAC-2004, R. May and A. J. Roberts, Eds, ANZIAM, p.786–804, 46*
Grazier K. R., Newman W. I., Sharp P. W., 2008, *American Astronomical Society, DDA meeting*
Grazier K. R., Newman W. I., Varadi F., Kaula W. M., Hyman J. M., 1999, *ICARUS 140, p.353–368, 2*
Grazier K. R., Newman W. I., Sharp P. W., 2013, *The Astronomical Journal, p.112–119, 145*
Rehman S., 2013, *AJCM, p.195–204, 3*
Duncan M. J., Levison H. F., Lee M. H., 1998, *AJ, p.2067–2077, 116*
Sharp P. W., Qureshi M. A., 2013, *Numerical Algorithms, p.133–148, 62*
Kirsh D. R., Duncan M., Brasser R., Levison H. F., 2009, *ICARUS 199, p.197–209, 1*
Hairer E., Nørsett S. P., Wanner G., 1993, *Springer, second edition*
Levison H. F., Duncan M., 1994, *ICARUS, p.18–36, 108*
Lykawka P. S., Horner J., Jones B. W., Mukai T., 2009, *Monthly Notices of the Royal Astronomical Society 398, p.1715–1729, 4*
Minton D. A., Malhotra R., 2010, *ICARUS 207, p.744–757, 2*
Murray C. D., Dermott S. F., 1999, *Cambridge University Press, UK*
Tiscareno M. S., Malhotra R., 2009, *The Astronomical Journal, p.18–36, 3*
Williams D. R., 2019, *http://nssdc.gsfc.nasa.gov/planetary/factsheet/; last accessed November, 2019*
Rehman S., 2014, *American Journal of Computational Mathematics, p.446–454, 4*
Candy J., 1991, *Celestial mechanics and Dynamical astronomy, p.221–240, 52*
Hairer E., Lobich C., Wanner G., 2002, *Springer-Verlag, New York*